Journal of Electronic Research and Application, 2026, Volume 10, Issue 5
http://ojs.bbwpublisher.com/index.php/JERA
Online ISSN: 2208-3510
Print ISSN: 2208-3502

Study on the Handling Stability of Intelligent Driving Vehicles under High-Speed Conditions Based on Nonlinear Models

Ziang Wu[1], Bing Huo[1,2]*, Yier Lin[1,2]

[1]School of Mechanical Engineering, Tianjin University of Science and Technology, Tianjin 300222, China
[2]Tianjin Key Lab of Integrated Design and On-line Monitoring for Light Industry & Food Machinery and Equipment, Tianjin 300222, China

***Corresponding author:** Bing Huo, huobing@tust.edu.cn

Abstract: Nonlinear Model Predictive Control (NMPC) has attracted growing attention in vehicle motion control. This paper proposes an NMPC-based trajectory tracking controller for autonomous vehicles that incorporates body roll dynamics to mitigate the accuracy loss and instability caused by increased nonlinearities during high-speed cornering. Using Newton's second law and vehicle kinematics, and considering body roll geometry together with load transfer effects, a nonlinear vehicle dynamics model is established, comprising vehicle body dynamics and an improved "Magic Formula" tyre model. On this basis, an NMPC predictive model with appropriate linear and nonlinear constraints is developed to keep the vehicle's operating states within a feasible region. Co-simulations on a CarSim-Simulink platform under high-speed cornering and double lane-change scenarios show that the proposed controller effectively improves trajectory tracking accuracy and vehicle state stability.

Keywords: High-speed turning; Nonlinear Model Predictive Control (NMPC); Stability control; Vehicle dynamics; Trajectory tracking

Online publication: Jun 29, 2026

1. Introduction

Autonomous driving has evolved rapidly in the past decade, and trajectory tracking has emerged as one of its fundamental control problems, directly affecting driving safety, comfort, and energy efficiency [1]. Early studies adopted linear single-track models together with classical controllers such as PID or linear quadratic regulators to obtain steering commands that drive the lateral error toward zero. Model predictive control (MPC) later became mainstream because it explicitly handles state and actuator constraints during receding-horizon optimisation, which is particularly attractive for safety-critical driving tasks [2].

Most of the linear MPC schemes in the literature use a bicycle model with a constant longitudinal speed and treat only the lateral velocity and yaw rate as control objectives [3]. This simplification works well in low-speed and moderate-curvature conditions, but breaks down when the vehicle operates close to its handling limits. Under aggressive manoeuvres, the tyre lateral force leaves its linear region, large load transfer develops across the axles, and the body roll dynamics can no longer be neglected [4]. To address these issues, several researchers have extended the bicycle model with additional degrees of freedom and nonlinear tyre representations [5]. For example, an adaptive MPC that estimates tyre cornering stiffness and road friction online has been shown to outperform fixed-parameter MPC in varying operating conditions, and a modified vehicle kinematic model with a steering angle correction function has been reported to reduce the double-lane-change tracking error by more than 70% on a CarSim–Simulink platform [6].

The coupling between tyre forces and roll dynamics is strongly nonlinear, which makes nonlinear model predictive control (NMPC) a natural choice. Yahya *et al.* developed an eight-state NMPC formulation that integrates rollover prevention with lateral stability and traction control for very-high-speed applications. Chen *et al.* introduced a cascaded discretisation scheme that preserves accuracy at the beginning of the prediction horizon while reducing computational cost further ahead, and demonstrated improved stability on low-adhesion roads at high speed [7]. Data-driven variants have also been explored: a recurrent high-order neural network model can capture nonlinear vehicle dynamics for torque-vectoring stabilization [8]. In parallel, linear-parameter-varying formulations have been used to retain part of the computational efficiency of linear MPC while tracking high-curvature references in real time [9]. The widespread use of the Pacejka "Magic Formula" tyre model in these works underlines the importance of an accurate tyre-ground representation for any high-speed stability controller [10].

In spite of these advances, most existing NMPC schemes for trajectory tracking either assume a constant longitudinal speed or neglect body-roll motion, so the accuracy loss caused by simultaneous lateral and roll nonlinearities during high-speed cornering has not been fully addressed. This paper therefore proposes an NMPC-based trajectory tracking controller that takes both the front-wheel steering angle and the longitudinal acceleration as control inputs and explicitly integrates body-roll dynamics into an eight-dimensional state-space prediction model.

2. Establishment of a vehicle model considering the front-wheel steering angle

2.1. Vehicle dynamics model

During cornering, roll motion induces load transfer and amplifies system nonlinearities. The front wheels may also slip under extreme conditions. To capture these effects, an eight-degree-of-freedom (DOF) full-vehicle dynamics model is established in a global coordinate system. The DOFs comprise longitudinal and lateral displacements, yaw and roll of the vehicle body, and the spin of each of the four wheels. The vehicle is further decomposed into sprung and unsprung masses to analyse roll motion and the dynamic variation of tyre vertical loads.

The main modelling assumptions are as follows. (i) Roll-centre heights are equal and constant at both axles. (ii) Ackermann steering geometry holds. (iii) Rotational and translational motions of the unsprung mass are decoupled. (iv) The sprung-mass centre of gravity coincides with the whole-vehicle centre of gravity. (v) Tyres remain perpendicular to the ground without vertical deformation. (vi) No wheel lift-off occurs. (vii) Oscillatory roll of the sprung mass is neglected. The schematic of longitudinal, lateral, and yaw motions is shown in **Figure 1(a)**. The roll model is illustrated in **Figure 1(b)**.

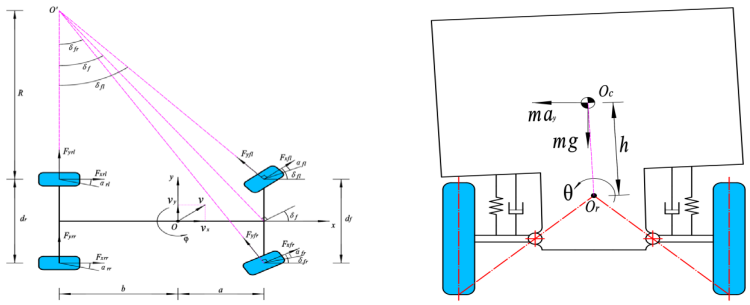

(a)Vehicle dynamics model (b)Vehicle roll model

Figure 1. Vehicle dynamics model.

From the geometry, the steering angles δ_{fl} and δ_{fr} of the left and right front wheels are obtained from the steering-wheel angle, the steering transmission ratio, and the front-axle geometry. The longitudinal and lateral kinematic equations relate vehicle accelerations to velocities through the yaw rate r. The complete set is given in **Equation (1)**:

$$\begin{cases} \delta_{fl} = \arctan\left[\dfrac{2(a+b)\tan\delta_f}{2(a+b)-d_f\tan\delta_f}\right] \\ \delta_{fr} = \arctan\left[\dfrac{2(a+b)\tan\delta_f}{2(a+b)+d_f\tan\delta_f}\right] \\ \delta_f = \dfrac{\delta_{sw}}{i_{sw}} \\ a_x = \dot{v}_x - v_y r, \quad a_y = \dot{v}_y + v_x r \end{cases} \tag{1}$$

Here δ_f is the equivalent front-axle steering angle; δ_{sw} is the steering-wheel angle; i_{sw} is the steering transmission ratio; a and b are the distances from the centre of gravity (CG) to the front and rear axles; d_f is the front-axle track width; a_x and a_y are the longitudinal and lateral accelerations; and v_x, v_y are the longitudinal and lateral velocities.

The longitudinal and lateral motions are driven by tyre–ground forces and are coupled with the yaw rate and the roll motion of the sprung mass. The yaw motion about the z-axis arises from moments produced by tyre forces and from inertial contributions of the unsprung-mass accelerations. The roll motion about the x-axis is driven by tyre reaction forces, suspension forces, and the inertial force of lateral acceleration acting at the roll centre. These four balance equations are collected in **Equation (2)**:

$$\begin{cases} ma_x = \left(F_{xfl}\cos\delta_{fl} + F_{xfr}\cos\delta_{fr}\right) - \left(F_{yfl}\sin\delta_{fl} + F_{yfr}\sin\delta_{fr}\right) + F_{xrl} + F_{xrr} \\ ma_y = \left(F_{yfl}\cos\delta_{fl} + F_{yfr}\cos\delta_{fr}\right) + \left(F_{xfl}\sin\delta_{fl} + F_{xfr}\sin\delta_{fr}\right) + F_{yrl} + F_{yrr} \\ I_z\ddot{\psi} = \frac{d_f}{2}\left(F_{xfr}\cos\delta_{fr} - F_{xfl}\cos\delta_{fl} + F_{yfl}\sin\delta_{fl} - F_{yfr}\sin\delta_{fr}\right) \\ + a\left(F_{xfr}\sin\delta_{fr} + F_{xfl}\sin\delta_{fl} + F_{yfr}\cos\delta_{fr} + F_{yfl}\cos\delta_{fl}\right) + \frac{d_r}{2}(F_{xrr} - F_{xrl}) - b\left(F_{yrr} + F_{yrl}\right) \\ I_x\ddot{\theta} = I_{xz}\ddot{\psi} + ma_y h_{rc} - C_\theta\dot{\theta} - K_\theta\theta + mgh_{rc}\theta \end{cases} \tag{2}$$

In Equation (2), F_{xij} and F_{yij} (with $i \in$ {fl, fr, rl, rr}) are the longitudinal and lateral tyre forces at each wheel; I_z and I_x are the moments of inertia about the z- and x-axes; I_{xz} is the product of inertia; θ and ψ are the roll and yaw angles; C_φ and K_φ are the roll damping and stiffness coefficients; h_{rc} is the distance from the CG to the roll centre; d_r is the rear-axle track width; and m is the total vehicle mass.

2.2. "Magic Formula" tyre model

Tyre-road interaction is highly nonlinear due to variations in tyre construction, materials, and friction conditions. It is the primary source of nonlinearity in vehicle dynamics [10]. The "Magic Formula" (MF) tyre model is therefore adopted. The MF model relates lateral force, longitudinal force, and aligning moment to slip angle, slip ratio, and adhesion coefficient. Only the longitudinal and lateral force components are used in this study. The general MF expression, together with the definitions of the longitudinal slip ratio *sx* and the tyre slip angle *α*, is given in **Equation (3)**:

$$\begin{cases} F = D_0 \sin\left\{C_0 \arctan\left[B_0 x - E_0\left(B_0 x - \arctan(B_0 x)\right)\right]\right\} \\ s_x = \begin{cases} \dfrac{\omega_w r_t - v_x}{\omega_w r_t}, & \omega_w r_t > v_x \\ \dfrac{\omega_w r_t - v_x}{v_x}, & \omega_w r_t < v_x \end{cases} \\ \alpha = \arctan\left(\dfrac{v_y}{v_x}\right) \end{cases} \tag{3}$$

Here B_0**,** C_0, D_0, E_0 are the stiffness, shape, peak, and curvature factors of the MF; ω_w is the wheel angular speed; and r_t is the effective rolling radius. A positive s_x corresponds to driving; a negative s_x corresponds to braking.

Under pure lateral slip, the lateral tyre force F_y is computed from **Equation (4)**:

$$\begin{cases} B_y = \dfrac{b_3 F_N^2 + b_4 F_N}{C_y D_y} e^{-b_5 F_N} \\ C_y = b_0 \\ D_y = b_1 F_N^2 + b_2 F_N \\ E_y = b_6 F_N^2 + b_7 F_N + b_8 \\ F_y = D_y sin\left\{C_y \arctan\left[B_y \alpha - E_y\left(B_y \alpha - \arctan(B_y \alpha)\right)\right]\right\} \end{cases} \tag{4}$$

In Equation (5), F_N is the normal tyre load.

The MF parameters used in this study are listed in **Table 1**. They correspond to a representative passenger-car tyre on dry asphalt and satisfy the physical ranges recommended in. The shape factor *C* is close to 1.65 for the longitudinal direction and 1.30 for the lateral direction; the curvature factor *E* is bounded in the interval (−2, 1).

Table 1. Magic Formula parameter values

Parameter	Value	Parameter	Value
B_x	10.0	B_y	8.5
C_x	1.65	C_y	1.30
D_x	1335 N	D_y	1215 N
E_x	0.97	E_y	−0.10
a_0	1.65	a_1	−6.5
a_2	1100	a_3	1100
a_4	10.0	a_5	0.0
a_6	−0.003	a_7	0.20
a_8	0.003	a_9	0.03

Tyre vertical loads vary continuously during motion. Under high-speed lane changes, roll-induced load transfer cannot be ignored. Both static and dynamic load components must therefore be incorporated into the MF model. The tyre force diagram is shown in **Figure 2**.

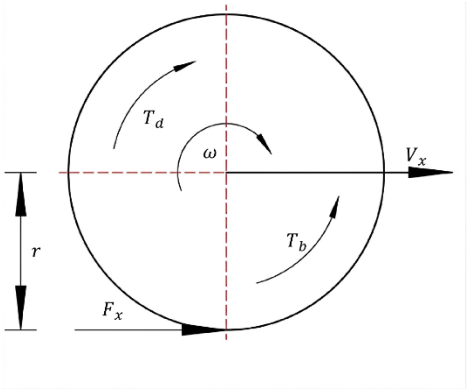

Figure 2. Tyre force diagram.

The rotational dynamics of the four wheels are described by **Equation (5)**. The braking and driving torques are kept distinct for each wheel:

$$\begin{cases} I_t\dot{\omega}_{fl} = -F_{xfl}r_t - T_{bfl} \\ I_t\dot{\omega}_{fr} = -F_{xfr}r_t - T_{bfr} \\ I_t\dot{\omega}_{rl} = -F_{xrl}r_t - T_{brl} + T_{drl} \\ I_t\dot{\omega}_{rr} = -F_{xrr}r_t - T_{brr} + T_{drr} \end{cases} \tag{5}$$

Here I_t **is** the wheel moment of inertia; T_{bij} is the braking torque at each wheel; and T_{drl} , T_{drr} are the driving torques on the rear wheels.

Assuming longitudinal symmetry, the static tyre vertical loads at the four wheels are given by **Equation (6)**:

$$\begin{cases} F_{zfl} = mg\dfrac{b}{l} - ma_x\dfrac{h_g}{l} - ma_y\dfrac{h_g}{d_f}\cdot\dfrac{b}{l}, & F_{zfr} = mg\dfrac{b}{l} - ma_x\dfrac{h_g}{l} + ma_y\dfrac{h_g}{d_f}\cdot\dfrac{b}{l} \\ F_{zfl} = mg\dfrac{b}{l} - ma_x\dfrac{h_g}{l} - ma_y\dfrac{h_g}{d_f}\cdot\dfrac{b}{l}, & F_{zfr} = mg\dfrac{b}{l} - ma_x\dfrac{h_g}{l} + ma_y\dfrac{h_g}{d_f}\cdot\dfrac{b}{l} \end{cases} \tag{6}$$

Here $l = a + b$ is the wheelbase, and h_g is the CG height above the ground.

Assuming that the rear wheels do not steer ($\delta_{rl} = \delta_{rr} = 0$), the four wheel slip angles are given by **Equation (7)**:

$$\begin{cases} \alpha_{fl} = \delta_{fl} - \arctan\dfrac{v_y + a\dot{\psi}}{v_x - \dfrac{d_f}{2}\dot{\psi}}, & \alpha_{fr} = \delta_{fr} - \arctan\dfrac{v_y + a\dot{\psi}}{v_x + \dfrac{d_f}{2}\dot{\psi}} \\ \alpha_{rl} = \arctan\dfrac{v_y - b\dot{\psi}}{v_x - \dfrac{d_r}{2}\dot{\psi}}\left(\delta_{rl} = 0\right), & \alpha_{rr} = \arctan\dfrac{v_y - b\dot{\psi}}{v_x + \dfrac{d_r}{2}\dot{\psi}}\left(\delta_{rr} = 0\right) \end{cases} \tag{7}$$

The longitudinal velocity at each wheel centre is given by **Equation (8)**:

$$\begin{cases} v_{xfl} = \left(v_x - \dfrac{d_f}{2}\dot{\psi}\right)\cos\delta_{fl} + \left(v_y + a\dot{\psi}\right)\sin\delta_{fl} \\ v_{xfr} = \left(v_x + \dfrac{d_f}{2}\dot{\psi}\right)\cos\delta_{fr} + \left(v_y + a\dot{\psi}\right)\sin\delta_{fr} \\ v_{xrl} = v_x - \dfrac{d_r}{2}\dot{\psi}, v_{xrr} = v_x + \dfrac{d_r}{2}\dot{\psi} \end{cases} \tag{8}$$

The dynamic load transfers between the front and rear axles caused by lateral acceleration are given by **Equation (9)**:

$$\begin{cases} \Delta F_{zf} = \dfrac{m_s a_y K_f h_{rc} l_r}{d_f\left(K_f + K_r\right)l - m_s g h_{rc} l_r} + \dfrac{m_s a_y h_f}{d_f} \\ \Delta F_{zr} = \dfrac{m_s a_y K_r h_{rc} l_f}{d_r\left(K_f + K_r\right)l - m_s g h_{rc} l_f} + \dfrac{m_s a_y h_r}{d_r} \end{cases} \tag{9}$$

Here K_f **and** K_r are the front and rear suspension roll stiffnesses; h_f and h_r are the heights of the front and rear roll centres; l_f and l_r are the distances from the CG to the front and rear roll centres; and m_s is the sprung mass.

Substituting the updated vertical load $F_N = F_{Zij} + \Delta F_Z$ into the MF coefficients yields the modified MF lateral force for extreme operating conditions, given in **Equation (10)**:

$$F_y = D_y \sin\left\{C_y \arctan\left[B_y\alpha - E_y\left(B_y\alpha - \arctan(B_y\alpha)\right)\right]\right\} \tag{10}$$

3. NMPC controller design

An NMPC controller is designed based on the nonlinear vehicle model established above. The design follows the four standard MPC components, prediction model, constraints, cost function, and solver. Additional nonlinear constraints are introduced to limit body roll and excessive steering.

3.1. Prediction model

Decoupling the time derivatives of the state variables yields the continuous-time state-space form. The eight-dimensional state vector covers roll, yaw, longitudinal and lateral velocities, and global-frame position. The two-dimensional control input contains the front-wheel steering angle and the desired longitudinal velocity. The complete prediction model is given in **Equation (11)**:

$$\begin{cases} \dot{\boldsymbol{t}} = f\left(\xi, u\right) \\ \xi = \begin{bmatrix} \theta & \dot{\theta} & \psi & \dot{\psi} & v_x & v_y & X & Y \end{bmatrix}^T \\ u = \begin{bmatrix} \delta_f & v_x \end{bmatrix}^T \end{cases} \tag{11}$$

3.2. Constraints

Physical and safety limits are imposed as box-type and nonlinear inequality constraints. They cover the longitudinal velocity, longitudinal acceleration, steering angle, steering rate, roll angle, roll rate, and the four-wheel vertical loads. The complete set of constraints is given in **Equation (12)**:

$$\begin{cases} 0 \le v_x \le 160\ km/h, -0.615 \le a_x \le 0.615\ m/\mathrm{s}^2 \\ -0.85 \le \dot{\theta} \le 0.85\ rad/s, -25°/s \le \dot{\delta}_f \le 25°/s \\ -25° \le \delta_f \le 25°, -25°/s \le \dot{\delta}_f \le 25°/s \\ F_{z,l} \le F_z \le F_{z,u} \end{cases} \tag{12}$$

The roll-angle and steering-rate bounds prevent rollover and excessive actuator demand.

3.3. Cost function

The continuous model is discretised by the Euler method with sampling interval *Ts*. The discrete-time prediction model and the standard receding-horizon assumption are given in **Equation (13)**:

$$\begin{cases} x\left(k+1\right) = f\left(x\left(k\right), u\left(k\right)\right), \quad k \ge 0 \\ u\left(k+i\right) = u\left(k+N_c-1\right), \quad i = N_c, N_c+1, \ldots, N_p-1 \\ x\left(k+i+1\right) = x\left(k+i\right) + T_s \cdot f\left(x\left(k+i\right), u\left(k+i\right)\right) \\ u\left(k+i\right) = u\left(k+i-1\right) + \Delta u\left(k+i\right) \end{cases} \tag{13}$$

Here *Np* **is** the prediction horizon length and $Nc \le Np$ is the control horizon length. Outside the control horizon, the input is held constant.

The cost function combines tracking-error penalties with a control-smoothness term, as listed in **Equation (14)**:

$$\begin{cases} J_1 = \sum_{i=1}^{N_p} \left[v_x(k+i \mid k) - v_{x,\text{ref}}(k+i \mid k) \right]^2, J_2 = \sum_{i=1}^{N_p} \left[X(k+i \mid k) - X_{\text{ref}}(k+i \mid k) \right]^2 \\ J_3 = \sum_{i=1}^{N_p} \left[Y(k+i \mid k) - Y_{\text{ref}}(k+i \mid k) \right]^2, J_4 = \sum_{i=1}^{N_p} \left[\psi(k+i \mid k) - \psi_{\text{ref}}(k+i \mid k) \right]^2 \\ J_5 = \sum_{i=1}^{N_c} \left[\Delta\delta_f(k+i)^2 + \Delta a_x(k+i)^2 \right] \end{cases} \quad (14)$$

In **Equation (14)**, J_1 penalises the longitudinal velocity error; J_2 and J_3 penalise position errors in the X and Y directions; J_4 penalises the heading-angle error; and J_5 penalises control increments to ensure smooth steering and acceleration. The total cost is the weighted sum $J = w_1J_1 + w_2J_2 + w_3J_3 + w_4J_4 + w_5J_5$, with positive weights w_1–w_5 tuned for the driving scenario.

4. Simulation and analysis

A CarSim-Simulink co-simulation is built to verify the proposed NMPC algorithm. The setup follows the standard procedure used in previous NMPC studies. Simulink hosts the NMPC controller in a MATLAB Function block. CarSim provides the high-fidelity vehicle model. The main vehicle parameters are listed in **Table 2**.

Table 2. Vehicle parameters

Parameter	Symbol	Unit	Value
Vehicle mass	m	kg	1400
Distance from CG to front axle	a	m	1.103
Distance from CG to rear axle	b	m	1.892
Moment of inertia about x-axis	I_x	kg·m²	536
Distance from CG to roll centre	h	m	0.39
Roll damping coefficient	C_φ	N·m·s/rad	4500
Roll stiffness	K_φ	N·m/rad	80000

4.1. Double lane-change simulation without disturbance

A double lane-change reference trajectory is generated by spline curves. The vehicle speed is held constant at 60 km/h. The results are shown in **Figure 3**.

Figure 3(a) shows that the improved NMPC achieves substantially higher lateral-position accuracy throughout the manoeuvre. The lateral error remains within a very small range. The conventional NMPC, in contrast, cannot eliminate this error effectively. **Figure 3(b)** shows that the improved accuracy is achieved through more active front-wheel steering. The steering-angle variations are larger, but they remain smooth.

Figures 3(c) and **3(d)** confirm that both the longitudinal-speed tracking error and the yaw-angle tracking error are markedly smaller under the improved NMPC.

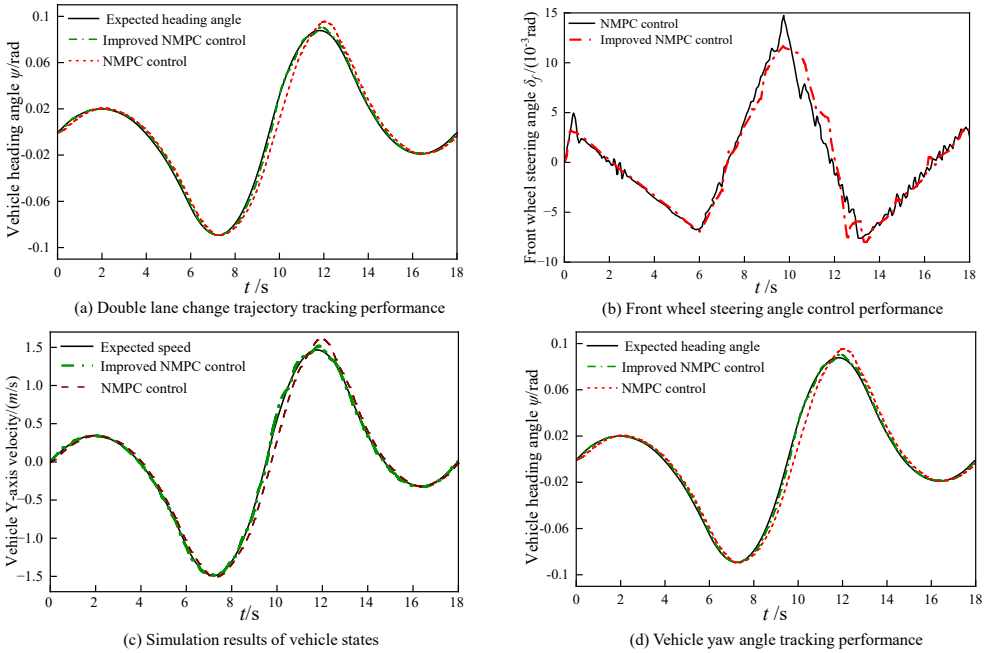

(a) Double lane change trajectory tracking performance

(b) Front wheel steering angle control performance

(c) Simulation results of vehicle states

(d) Vehicle yaw angle tracking performance

Figure 3. Simulation of dual-line shifting operation.

4.2. High-speed simulation under disturbances

To evaluate robustness, perception disturbances are simulated by adding band-limited white noise to the state feedback from CarSim. The results are shown in **Figure 4**.

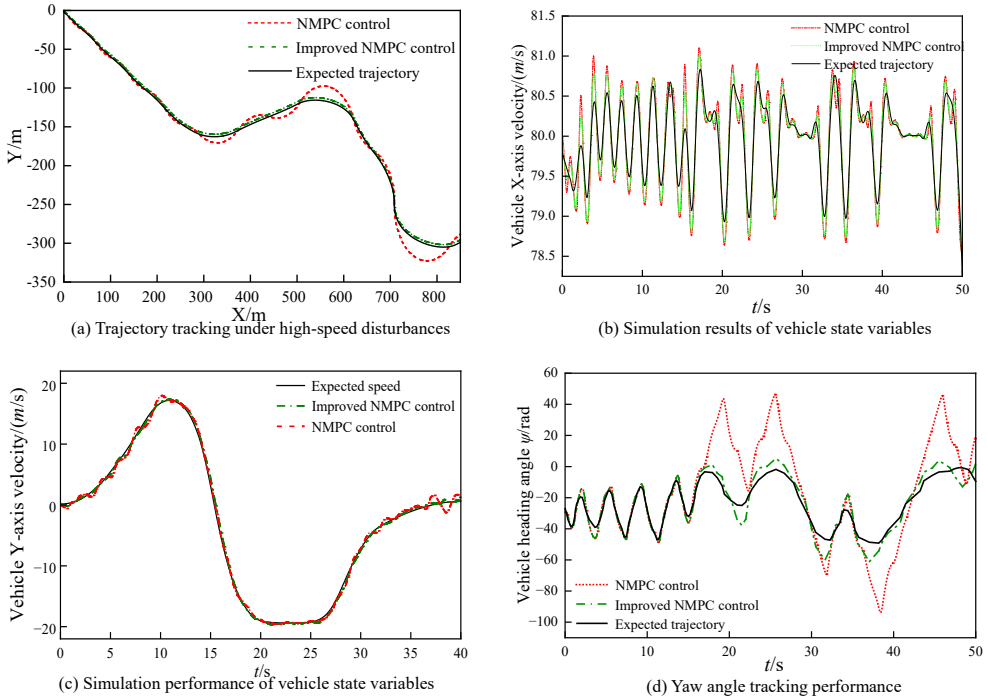

(a) Trajectory tracking under high-speed disturbances

(b) Simulation results of vehicle state variables

(c) Simulation performance of vehicle state variables

(d) Yaw angle tracking performance

Figure 4. High-speed lane change simulation.

Under disturbances, the conventional NMPC fails to filter the noise effectively. It produces large fluctuations in both speed and yaw tracking, as visible in **Figures 4(b)** and **4(d)**. The improved NMPC keeps these errors within a much narrower range. It also produces smoother cornering trajectories, as shown in **Figure 4(a)**. Similar robustness advantages have been reported for data-driven NMPC and for LPV-NMPC .

The performance gap has a clear physical explanation. The conventional NMPC relies on linear assumptions, small-angle tyre approximations and a single-track vehicle representation. These assumptions amplify the controller's sensitivity to external disturbances. The improved NMPC, by contrast, accounts explicitly for roll stability, nonlinear tyre dynamics, and their coupling. It also enforces nonlinear stability constraints. This comprehensive nonlinear modelling enhances dynamic robustness and produces effective disturbance attenuation.

5. Conclusion

This paper proposes an NMPC algorithm for the integrated longitudinal and lateral trajectory tracking of autonomous vehicles. A vehicle model incorporating body-roll dynamics is established, combining Newton-based roll dynamics with a nonlinear coupled tyre model to capture roll behaviour and tyre coupling. Based on this model, a highly nonlinear prediction model with an eight-dimensional state vector is built and nonlinear constraints keep all states within a safe operating region. CarSim-Simulink co-simulations show that the proposed NMPC achieves accurate integrated longitudinal and lateral trajectory tracking with high accuracy and robustness across various high-speed scenarios.

Disclosure statement

The authors declare no conflict of interest.

References

[1] Paden B, Čáp M, Yong S, et al., 2016, A Survey of Motion Planning and Control Techniques for Self-Driving Urban Vehicles. IEEE Trans Intell Veh, 1(1): 33–55.

[2] Falcone P, Borrelli F, Asgari J, et al., 2007, Predictive Active Steering Control for Autonomous Vehicle Systems. IEEE Trans Control Syst Technol, 15(3): 566–580.

[3] Lin F, Chen Y, Zhao Y, et al., 2019, Path Tracking of Autonomous Vehicle Based on Adaptive Model Predictive Control. Int J Adv Robot Syst, 16(5): 1–14.

[4] Yahya J, Saha S, Xue H, et al., 2023, Model Predictive Control for Integrated Lateral Stability, Traction/Braking Control, and Rollover Prevention of Electric Vehicles, arXiv:2306.06096.

[5] Jeong Y, Yim S, 2021, Model Predictive Control–Based Integrated Path Tracking and Velocity Control for Autonomous Vehicle with Four-Wheel Independent Steering and Driving. Electronics, 10(22): 2812.

[6] Jin H, Duan C, Lu K, et al., 2023, Coupled Lateral and Longitudinal Trajectory Tracking Control with a Modified Vehicle Kinematics Model for Autonomous Vehicles. Intell Transp Infrastruct, 2(1): liad009.

[7] Chen H, Song Y, Liu K, et al., 2024, Efficient Nonlinear Model Predictive Path Tracking Control for Autonomous Vehicle: Investigating the Effects of Vehicle Dynamics Stiffness. Machines, 12(10): 742.

[8] Chen H, Zhang J, Lv C, 2022, RHONN Modelling-Enabled Nonlinear Predictive Control for Lateral Dynamics

Stabilization of an In-Wheel Motor Driven Vehicle, arXiv:2201.08558.

[9] Kumar N, Pachamuthu R, 2025, Real-Time LPV-Based Non-Linear Model Predictive Control for Robust Trajectory Tracking in Autonomous Vehicles, arXiv:2506.04684.

[10] Pacejka H, 2012, Tire and Vehicle Dynamics (3rd ed.), Butterworth-Heinemann, Oxford.